A new approach to variable-topology shape design using a constraint on perimeter

R. B. Haber

Department of Theoretical and Applied Mechanics, University of Illinois at Urbana-Champaign, Urbana, IL 61801, USA

C. S. Jog and M. P. Bendsøe

Mathematical Institute, Building 303, The Technical University of Denmark, DK-2800 Lyngby, Denmark

Abstract

This paper introduces a method for variable-topology shape optimization of elastic structures called the *perimeter method.* An upper-bound constraint on the perimeter of the solid part of the structure ensures a well-posed design problem. The perimeter constraint allows the designer to control the number of holes in the optimal design and to establish their characteristic length scale. Finite element implementations generate practical designs that are convergent with respect to grid refinement. Thus, an arbitrary level of geometric resolution can be achieved, so single-step procedures for topology design and detailed shape design are possible. The perimeter method eliminates the need for relaxation, thereby circumventing many of the complexities and restrictions of other approaches to topology design.

1 Introduction

A number of effective procedures for shape optimization of elastic structures are available; some are implemented in commercial finite element software systems and are in routine use in industry. Typically, these procedures do not admit changes in the connectivity of the structure's geometry. Instead, shape modifications are described by moving the boundaries of the structural domain. These *fixed-topology* shape optimization procedures impose a significant constraint on the design -- it is not possible to create new boundaries or to remove existing ones by adding or deleting holes. In recent years, new techniques for *variable-topology* shape optimization problems have been introduced. [These problems are sometimes called *generalized* shape optimization problems (Rozvany 1993).] In these methods, holes may be added or deleted to modify the connectivity of the structure during the course of the optimization process. This added flexibility can yield

significant weight reductions or improved performance relative to fixed-topology designs. Thus, there is considerable interest in developing mathematical theory and computational methods to address this class of problems.

Fig. 1 illustrates a typical variable-topology shape design problem. A fixed amount of elastic material is to be distributed within a candidate design domain. The objective is to minimize the structural compliance for a specified set of loads and supports. No restrictions are placed on the connectivity of the solid region Ω_s. Unfortunately, it turns out that this design problem is not well posed, see for example (Tartar 1977; Murat 1977; Lurie et al. 1982; Murat and Tartar 1985; Kohn and Strang 1986). In particular, we typically can construct a *nonconvergent* sequence of designs such that the compliance reduces monotonically. Therefore, an optimal design does not exist.

To illustrate, suppose we are given a design that satisfies the volume constraint. In general, a design with the same volume and lower compliance can be obtained by increasing the number of holes. We can continue to reduce the compliance by generating new designs with more holes. Eventually, this leads to "chattering" designs with microscopic perforations, a result first observed numerically by Cheng and Olhoff (1981) in the analogous variable-thickness Kirchhoff plate design problem. The design tends toward a configuration with an unbounded number of microscopic holes, rather than a finite number of macroscopic holes.

There are two alternatives for generating a well-posed, variable-topology optimization problem; one must either explicitly include chattering solutions in the problem formulation or take steps to ensure that they do not occur. In the former option, a procedure called *relaxation* accomodates chattering designs by first extending the design space to include materials with periodic, perforated microstructures and then using homogenization theory to compute effective material properties (Lurie et al. 1982; Kohn and Strang 1986; Goodman et al. 1986; Gibianski and Cherkaev 1987). This approach, often called the *homogenization method* for topology optimization, has been extensively developed in recent years. The second option involves restricting the design space to exclude chattering designs (Haber, Jog and Bendsøe 1994). This is the basis of the new variable-topology design method presented in this paper.

The homogenization method has some attractive features. First, solutions to the relaxed problem are guaranteed to exist (Allaire and Kohn 1993a). The homogenization method also eliminates many (if not all) of the local extrema that occur in the macroscopic topology design problem, because relaxation is mathematically equivalent to a quasiconvexification operation (Kohn and Strang 1986; Kohn 1991). A number of finite element procedures for solving the relaxed problem appear in the literature (Bendsøe and

Kikuchi 1988; Allaire and Francfort 1993; Allaire and Kohn 1993; Bendsøe, Diaz and Kikuchi 1993; Jog, Haber and Bendsøe 1993, 1994).

When there are no *a priori* restrictions on the configuration of the microstructure and in the absence of an explicit penalty on intermediate volume fractions, homogenization methods commonly generate optimal designs with perforated microstructures. This is consistent with the expected form of continuum solutions to the relaxed problem. Unfortunately, it is often impractical to manufacture designs with perforated microstructures. When the design is required to include only macroscopic holes, the relaxed optimization problem does not lead directly to useful designs. Nonetheless, the relaxed solution still provides a useful bound on the compliance that can be achieved through variable-topology design. It might also suggest an effective macroscopic configuration to an experienced designer.

Consider the relaxed solution shown in Figs. 3 and 4 for the candidate region and loading shown in Fig. 2a. The prescribed volume of material is 20% of the volume of the candidate domain. Fig. 3 shows the optimal bulk density distribution and Fig. 4 shows the orientation and relative layer densities of the microstructure (see (Jog, Haber and Bendsøe 1994) for details of the rank-2 microstructure model used in this study). The design can be understood as a (half) bicycle wheel with an infinite number of tensioned spokes. The spokes are represented in the relaxed solution by perforated material with a radial, uniaxial microstructure. Although it is not possible to fabricate a wheel with an infinite number of spokes or to replicate the biaxial microstructures that appear in the transition region between the spokes and the "rim" of dense material, there are practical approximations to this design. For example, a conventional bicycle wheel with many wire spokes or a disk with a number of cutouts, as shown in Fig. 5, are practical realizations of the relaxed solution. A solid wheel, constructed of fiber-reinforced composite materials, is another practical interpretation that is sometimes used in professional racing bicycles.

Although relaxed solutions containing perforated microstructures might convey useful information, they do not directly address the macroscopic design problem illustrated in Fig. 1. Therefore, it is worthwhile to consider modifications to the relaxed formulation that suppress perforated material in the optimal design. The suppression can be achieved either by introducing an explicit penalty on intermediate values of the bulk density or by introducing *a priori* restrictions on the microstructural configuration (this constitutes a *partial* relaxation). Allaire and Kohn (1993) and Allaire and Francfort (1993) present solutions based on explicit penalties that are relatively free of perforated material. A restriction of the microstructure configuration to square holes in square, periodic cells is a common example of a partial relaxation; see for example (Bendsøe and Kikuchi 1988;

Susuki and Kikuchi 1991; Rodrigues and Fernandes 1994). Allaire and Kohn (1993) and Bendsøe, Diaz and Kikuchi (1993) point out that certain partial relaxations define effective stiffness properties that generate an implicit penalty on intermediate values of the bulk density. This explains why some partial relaxations generate designs that are mostly free of perforated material. In view of their similar properties, we refer to homogenization methods that are based either on a partial relaxation or on a full relaxation with an explicit penalty on intermediate densities as *penalized homogenization methods.*

Penalized homogenization formulations are not without problems. In particular, they revert to the original ill-posed integer design problem, in the limit, as the penalty forces the volume of perforated material to zero. Thus, the existence of a continuum solution is not assured. Although useful results might be obtained on a fixed grid, finite element solutions based on these methods are not convergent with respect to grid refinement. Nonconvergent behavior is to be expected, since it is possible to resolve the geometries of a compliance-minimizing sequence of designs (with an increasing number of holes) as the grid is refined. The suppression of local extrema that is obtained with a complete relaxation is also sacrificed in the penalized methods. Thus, the benefits of a full relaxation are not retained in the penalized homogenization methods. Indeed, less complicated formulations appear to perform equally well. Rozvany (1993) reports results obtained with a variable-thickness model (without microstructure) that are comparable in quality to those obtained with penalized homogenization methods.

Two other approaches to the variable-topology optimization problem are worthy of mention. These include the *bubble method* (Eschenauer et al., 1994), which iteratively introduces new holes and applies fixed-topology shape optimization algorithms in a hierarchical algorithm. The *engineering approach* replaces χ with a continuous density variable and introduces a penalty against intermediate densities to approximate the integer problem (Bendsøe, 1989; Rozvany, 1993; Mlejnek, 1992). This approach may yield useful engineering solutions when implemented on a fixed numerical grid. However, it does not directly address the ill-posedness of the underlying continuum problem, and solutions are often mesh-dependent. The properties of the engineering approach are not unlike those of penalized homogenization methods.

The remainder of this paper presents a new approach to topology optimization called the *perimeter method.* In contrast to homogenization methods, which expand the design space to include chattering designs, the perimeter method restricts the solution space to exclude chattering designs. An upper-bound constraint on the perimeter of the solid region enforces this restriction. The perimeter constraint leads to a well-posed continuum optimization problem for which solutions, comprised exclusively of of solid material and

void, are guaranteed to exist (Ambrosio and Buttazzo, 1993). There is no need to consider perforated microstructures or to apply homogenization theory, since geometric features with microscopic length scales are specificly excluded in the statement of the optimization problem. It is worth noting that other means, besides the present perimeter control approach, can be used to exclude chattering solutions from the design space. For example, image processing filters can be applied to bound the smallest length scale in the optimal geometry (Sigmund, 1995).

We present a finite element solution procedure based on the new formulation which offers a number of advantages over previous methods: 1) the new method is convergent with respect to grid refinement, so it can be used for detailed shape design as well as preliminary conceptual design; 2) the designer is able to establish a characteristic length-scale for holes, thereby controling the number of holes in the design; 3) the method is compatible with any design objective (it is not limited to compliance minimization) and general forms of design and response constraints; 4) the new procedure can be implemented with standard finite element analysis and optimization software.

The following section presents the continuum formulation of the topology optimization problem with a perimeter constraint, in both integer and continuous formats. Section 3 is concerned with the formulation and solution of the discrete optimization problem in a finite element setting. Numerical examples illustrating the capabilites of the perimeter method appear in Section 4. Section 5 presents conclusions and directions for future work.

2 A topology optimization problem with a constraint on perimeter

This section introduces a variable-topology shape optimization problem that uses a perimeter constraint to exclude chattering solutions from the feasible design space. We begin with a statement of the basic optimization problem diagrammed in Fig. 1, and then show how a perimeter constraint eliminates chattering designs to ensure a well-posed problem. The optimization problem is first formulated as an integer programming problem. Then a continuous approximation of the integer problem is introduced that is more tractable for numerical implementation.

Formulation of the basic variable-topology design problem

Consider the problem of finding the stiffest (minimum compliance) structure under a single loading condition that can be obtained by distributing a fixed volume $\overline{V}$ of homogeneous, isotropic, linear elastic material within a two-dimensional candidate domain

Ω with boundary $\Gamma = \overline{\Gamma_u \cup \Gamma_t}$ (see Fig. 1). No restriction is placed on the connectivity of $\Omega_S \subset \Omega$, the solid part of Ω where material is present. Let $\overline{\mathbf{C}}$ designate the elasticity tensor of the solid isotropic material. We introduce the indicator function,

$$\chi: \Omega \to \{0,1\} \text{ where } \chi(\mathbf{x}) = \begin{cases} 1 \text{ for } \mathbf{x} \in \Omega_S \\ 0 \text{ for } \mathbf{x} \in \Omega_V \equiv \Omega \setminus \Omega_S \end{cases}, \tag{1}$$

to represent arbitrary configurations of Ω_s. The region Ω_v is the portion of Ω occupied by void. The volume of the solid part of the structure is given by $\int_\Omega \chi d\Omega$, and the elasticity tensor in Ω is given by

$$\mathbf{C} = \chi \overline{\mathbf{C}}. \tag{2}$$

We now present the potential energy formulation of a small-deformation elasticity problem on Ω. Let $\mathbf{t}$, $\mathbf{b}$ and $\mathbf{u}$ denote surface traction, body force and displacement vectors. Also, let Γ_t and Γ_u be the traction and displacement boundaries of Ω, with boundary conditions $\mathbf{t} = \bar{\mathbf{t}}$ on Γ_t and $\mathbf{u} = \bar{\mathbf{u}}$ on Γ_u. An overbar denotes a prescribed quantity. We define the strain, the strain energy density, Cauchy's relation, the space of admissable displacement fields and the potential energy as

Bold

$$\boldsymbol{\varepsilon} = \frac{1}{2}\left[\nabla \mathbf{u} + (\nabla \mathbf{u})^t\right] \text{ in } \Omega, \tag{3}$$

$$W(\mathbf{C}, \boldsymbol{\varepsilon}) = \frac{1}{2}\boldsymbol{\varepsilon}^t \mathbf{C} \boldsymbol{\varepsilon} \text{ in } \Omega, \tag{4}$$

$$\mathbf{t} = (\mathbf{C}:\boldsymbol{\varepsilon}) \cdot \mathbf{n} \text{ on } \Gamma, \tag{5}$$

Bold

$$V_u \equiv \left\{\mathbf{u}: u_i \in H^1(\Omega); \mathbf{u} = \bar{\mathbf{u}} \text{ on } \Gamma_u\right\} \text{ and} \tag{6}$$

$$\Pi = \int_\Omega (W - \mathbf{b} \cdot \mathbf{u}) d\Omega - \int_{\Gamma_t} (\bar{\mathbf{t}} \cdot u) d\Gamma. \tag{7}$$

The stiffness problem is then stated as

$$\inf_{\mathbf{u}\in V_u} \Pi, \tag{8}$$

in which the elasticity tensor is given by equation (2) for a specified distribution of the indicator function χ.

The flexibility of an elastic structure is measured by the compliance,

$$J = \int_{\Gamma_t} (\bar{\mathbf{t}} \cdot \mathbf{u}) d\Gamma - \int_{\Gamma_u} (\mathbf{t} \cdot \bar{\mathbf{u}}) d\Gamma + \int_{\Omega} (\mathbf{b} \cdot \mathbf{u}) d\Omega. \tag{9}$$

According to Clapeyron's work theorem (Sokolnikoff, 1987), $J = -2\Pi$ when the displacement field solves the stiffness problem (8). Therefore, minimizing the compliance of a linear elastic structure with respect to design is equivalent to maximizing the potential energy subject to equation (8). We introduce the space of admissable indicator functions,

$$V_\chi \equiv \{\chi : \chi(\mathbf{x}) = 0 \text{ or } 1 \ \forall \mathbf{x} \in \Omega\}. \tag{10}$$

The stiffness version of the variable-topology, compliance optimization problem is stated as

$$\sup_{\substack{\chi\in V_\chi \\ \int_\Omega \chi d\Omega \le \bar{V}}} \ \inf_{\mathbf{u}\in V_u} \Pi. \tag{11}$$

The inner problem enforces equilibrium; the outer problem seeks an optimal design for minimum compliance. Problem (11) is a *macroscopic* topology design problem, since it does not include microstructure. It is an ill-posed problem, as explained above, due to a tendency to develop chattering designs.

The perimeter method

The new approach seeks to exclude chattering functions from the design space by limiting the design's perimeter. We define the perimeter of a design as the measure of the boundary of the solid region: $|\partial\Omega_s|$. The perimeter is equal to the total surface area of the boundary of Ω_s in three-dimensional problems, and to the total arc length of the boundary of Ω_s in two-dimensional problems. It is evident that the perimeter is a positive scalar function of the indicator function χ.

Fig. 6 illustrates how the perimeter constraint accomplishes the objective of excluding chattering designs. Designs with identical areas are perforated with holes of three different sizes. Both the number of holes and the total perimeter of the holes increase as the radius of the holes decreases. Thus, designs with low perimeter measures have fewer and larger holes than designs with high perimeter measures. Chattering designs have an infinite number of infinitely fine perforations, and are characterized by an infinite perimeter measure. Therefore, an upper bound constraint on the perimeter effectively excludes microscopic perforations and chattering solutions from the feasible design space. Further, the number and sizes of a finite set of holes can be controlled by limiting the perimeter without otherwise restricting the shape or layout of the holes.

In order to obtain a well-posed macroscopic topology design problem that excludes perforated material, we append to problem (11) an upper bound constraint on the perimeter,

$$\sup_{\substack{\chi \in V_\chi \\ \int_\Omega \chi \, d\Omega \le \overline{V} \\ |\partial\Omega_\chi| \le \overline{P}}} \inf_{u \in V_u} \Pi, \tag{12}$$

where $\overline{P}$ is a designer-specified value. Ambrosio and Buttazzo (1993) present an existence proof for a topology design problem similar to problem (12).

The use of the indicator function to represent the design configuration in problem (12) suggests that a raster geometry model, similar to a television image, could be used in numerical methods for solving the topology design problem. This is in contrast to the boundary-representation geometry models that are commonly used in finite element procedures for shape optimization. In the raster approach, a refined (often uniform) finite element grid covers the candidate design domain. A χ-value of either 0 or 1 is assigned to each element to define the design geometry. The boundaries of the solid region are represented implicitly by the element edges across which the value of χ changes. A raster geometry model is also an essential feature of numerical implementations of the homogenization approach to topology optimization.

The raster approximation of the continuum problem (12) leads to an integer programming problem that could be solved, in principle, by an appropriate global optimization strategy such as simulated annealing. However, raster geometry models generate optimization problems that are too large, and for which function evaluations are too expensive, to be solved directly in integer form. Therefore, we approximate problem (12) with a continuous programming problem to obtain a practical numerical method. The remainder of this paper deals with continuous approximations to (12). Since the form of

the approximation is not unique, it is important to keep in mind that problem (12) represents the basic statement of the new perimeter method for topology design. In particular, the existence proof of Ambrosio and Buttazzo provides the mathematical support for the perimeter method and any numerical method that derives from it.

Continuous approximations to the integer programming problem

We replace the indicator function χ with a distributed *interpolation parameter*, $\rho: \Omega \to [0,1]$ to achieve a continuous problem that is amenable to discrete solution methods. We have solid material where $\rho = 1$, and void wherever $\rho = 0$. Intermediate values of ρ indicate "transitional" material between solid and void. There is no particular physical significance to the transitional material, its only purpose is to provide a continuous optimization problem. Ultimately, we will introduce a penalty term to force ρ to its extreme values to approximate the integer problem (12). Thus, transitional material is supressed in the optimal design. New expressions in terms of ρ for the volume, perimeter and elasticity tensor are required. The volume is simply

$$V(\rho) = \int_{\Omega} \rho d\Omega. \tag{13}$$

We need a substitute for the perimeter measure $|\partial\Omega_s|$ that is compatible with the continuous interpolation model. The *total variation of* ρ is a suitable measure which approaches the perimeter, in the limit, as the amount of transitional material is forced to zero (Evans and Gariepy, 1992). In anticipation of a piecewise-continuous finite element discretization, we partition Ω into a set of open, disjoint regions Ω_α so that $\Omega = \overline{\bigcup_\alpha \Omega_\alpha}$. Let $V_\rho = \left\{\rho \in L_\infty(\Omega): \rho|_{\Omega_\alpha} \in H^1(\Omega_\alpha); 0 < \rho_{\min} \le \rho \le 1 \; \forall \mathbf{x} \in \Omega\right\}$, and recall that the total variation of a scalar function can be expressed as $TV(\rho) = \int_{\Omega \setminus \Gamma_J} |\nabla \rho| d\Omega + \int_{\Gamma_J} |\langle \rho \rangle| d\Gamma$ (Wheedon and Zygmund 1977). The lower bound $\rho_{\min}$ on the interpolation parameter ensures that W is positive definite. We use the total variation to express the "perimeter" of $\rho \in V_\rho$, accounting for the possibility that ρ may be discontinuous across sets of measure zero (e.g., the element boundaries).

$$P \equiv \int_{\Omega \setminus \Gamma_J} g_h(\nabla\rho,\xi)\,d\Omega + \int_{\Gamma_J} j(\langle\rho\rangle,\xi)\,d\Gamma;$$

$$g_h(\mathbf{w},\xi) \equiv \left[(1+2\xi)\mathbf{w}^T\mathbf{w} + \frac{\xi^2}{h^2}\right]^{1/2} - \frac{\xi}{h}; \tag{14}$$

$$j(r,\xi) \equiv \left[(1+2\xi)r^2 + \xi^2\right]^{1/2} - \xi$$

where $\Gamma_J = \Omega \setminus \bigcup_\alpha \Omega_\alpha$ is the jump set of ρ, $\langle\rho\rangle$ is the jump in ρ across Γ_J and h is a characteristic mesh dimension (e.g., the size of a finite element). The functions $g_h(\mathbf{w},\xi)$ and $j(r,\xi)$ are smooth approximations to $|\mathbf{w}|$ and $|r|$, respectively. The smoothing, based on the parameter ξ, circumvents numerical problems associated with the non-differentiability of the absolute value operators appearing in the expression for the total variation. Note that $\lim_{\xi\to 0} g_h(\nabla\rho,\xi) = |\nabla\rho|$ and $\lim_{\xi\to 0} j(\langle\rho\rangle,\xi) = |\langle\rho\rangle|$. Further, the approximations are exact in the limit of a discrete approximation to an integer design, even for $\xi > 0$. That is for all $\xi \geq 0$, $g_h(\nabla\rho,\xi) \to |\nabla\rho|$ as $|\nabla\rho| \to 0$ or $\frac{1}{h}$, and $j(\langle\rho\rangle,\xi) \to |\langle\rho\rangle|$ as $|\langle\rho\rangle| \to 0$ or 1.

The constitutive model given by equation (2) must be replaced by a continuous model consistent with the interpolation parameter ρ. The choice of the continuous constitutive model is not unique, and the model need not correspond to any specific physical system. It is only required that the model define a smooth interpolation between the elastic properties of the solid isotropic material and void. For example, one could use the simple relationship proposed by Bendsøe (1989) and Mlejnek (1992):

$$\mathbf{C} = \rho^p \overline{\mathbf{C}}; \quad p > 0. \tag{15}$$

If we select $p = 1$, then ρ can be interpreted as a variable-thickness parameter in two-dimensional problems. Alternatively, we can view ρ as an artificial density parameter in three-dimensional problems. We emphasize that these physical interpretations are extraneous to the proposed method. Interpolation models such as (15) are introduced here solely as continuous approximations to the integer problem (12), where there is no need for a physical interpretation for the conditions between solid material and void.

The optimized rank-2 microstructure model from the unpenalized homogenization method also provides a suitable interpolation for the constitutive model. Again, the details of the microstructural model and the fact that rank-2 microstructures are optimal for compliance design are not relevant in the perimeter-control method. Here we are only

interested in the fact that the effective properties of the rank-2 model define a continuous interpolation between the properties of solid material and void. One could also use the effective properties derived from a partial relaxation based on microstructures consisting of square holes in square cells (see, for example, (Bendsøe and Kikuchi, 1988)). We summarize here the effective properties of the optimized rank-2 model as described by Jog, Haber and Bendsøe (1994). The optimized rank-2 material model has three branches, identified by ρ, the Poisson ratio υ and the principal strain ratio, $k = \varepsilon_{II} / \varepsilon_{I}$. We use a secant stiffness relation in regions where there is uniaxial stress. The effective properties are isotropic and linear elastic:

$\frac{1+k}{1-\nu} < \rho \le 1$:

$$\mathbf{C} = \frac{E}{(1-\nu)(2-\rho+\nu\rho)} \begin{bmatrix} 1 & 1-\rho+\nu\rho & 0 \\ 1-\rho+\nu\rho & 1 & 0 \\ 0 & 0 & \frac{(1-\nu)\rho}{2} \end{bmatrix}$$

$\frac{1-k}{1+\nu} < \rho \le 1$:

$$\mathbf{C} = \frac{E}{(1+\nu)(2-\rho-\nu\rho)} \begin{bmatrix} 1 & \rho+\nu\rho-1 & 0 \\ \rho+\nu\rho-1 & 1 & 0 \\ 0 & 0 & \frac{(2-\rho-\nu\rho)}{2} \end{bmatrix}$$

$\rho < \min\left(\frac{1-k}{1+\nu}, \frac{1+k}{1-\nu}\right)$:

$$\mathbf{C} = \frac{\rho E}{(1-k)^2} \begin{bmatrix} 1 & -k & 0 \\ -k & 1 & 0 \\ 0 & 0 & \frac{(1+k)}{2} \end{bmatrix} \tag{16}$$

The elastic properties defined by the first two branches are identical to those of solid isotropic material for $\rho = 1$. The third branch is continuous with the first two at their common boundaries; it also gives $\mathbf{C} = \mathbf{0}$ for the void condition, $\rho = 0$.

We must ensure that intermediate values of ρ are suppressed in solutions to the continuous approximation of the integer design problem. This can be accomplished either by introducing an explicit penalty on intermediate values of ρ or by manipulating the

material model to obtain an implicit penalty. For example, we can specify $p > 1$ in equation (15) or use the effective properties from a partial relaxation to generate an implicit penalty. Alternatively, we can append a term to the compliance objective function that explicitly penalizes intermediate values of ρ. We follow the latter approach here.

In our current implementation, we use an optimality criterion method (see for example Jog, Haber and Bendsøe 1993 and 1994) to solve the design problem. This method is simplest for problems with a single equality constraint. Accordingly, we treat the constraint $P \le \overline{P}$ with an interior penalty method and enforce an equality constraint on the volume with a Lagrange multiplier method. We obtain the modified problem,

$$\sup_{\rho \in V_\rho} \inf_{\mathbf{u} \in V_u} \Pi + \alpha S_1 + \beta S_2 - \lambda \left[V(\rho) - \overline{V} \right], \tag{17}$$

in which α and β are positive scalars, S_1 is the penalty function that supresses intermediate values of ρ, S_2 is an interior penalty function for the constraint $P \le \overline{P}$ and λ is the Lagrange multiplier associated with the volume constraint.

A variety of choices are possible for the penalty functions S_1 and S_2. In the computational work reported here, they are given by

$$S_1 = \int_\Omega f \, d\Omega; \quad f(\rho) = \begin{cases} \dfrac{(\rho - \overline{\rho})^2}{2\overline{\rho}} & \text{for } 0 \le \rho \le \overline{\rho} \\ \dfrac{(\rho - \overline{\rho})^2}{2(1-\overline{\rho})} & \text{for } \overline{\rho} < \rho \le 1 \end{cases}; \qquad \overline{\rho} \equiv \frac{\overline{V}}{|\Omega|} \tag{18}$$

$$S_2 = \overline{P} \log\left[\overline{P} - P \right]. \tag{19}$$

Stationary conditions

The stationary conditions for the variational problem (17) give rise to the discrete stiffness equations and the optimization method described in the next section. The variational forms of the stationary conditions are given by

$$\int_\Omega \frac{\partial W}{\partial \boldsymbol{\varepsilon}} : \boldsymbol{\varepsilon}(\mathbf{v}) \, d\Omega = \int_\Omega \mathbf{b} \cdot \mathbf{v} \, d\Omega + \int_{\Gamma_t} \mathbf{t} \cdot \mathbf{v} \, d\Gamma \;\; \forall \mathbf{v} \in V_{u0}; \tag{20a}$$

$$\int_\Omega \frac{\partial W}{\partial \rho} q\,d\Omega + \alpha \int_\Omega \frac{df}{d\rho} q\,d\Omega + \beta \frac{dS_2}{dP}\left\{ \int_{\Omega \setminus \Gamma_J} \left[\frac{\nabla\rho^T \nabla q}{\left[\left(\nabla\rho^T \nabla\rho\right) + \frac{\xi^2}{h^2} \right]^{1/2}} \right] d\Omega + \int_{\Gamma_J} \left[\frac{\langle\rho\rangle\langle q\rangle}{\left(\langle\rho\rangle^2 + \xi^2 \right)^{1/2}} \right] d\Gamma \right\};$$

$$= \lambda \int_\Omega q\,d\Omega \;\forall q \in V_\rho \tag{20b}$$

in which $V_{u0} \equiv \left\{ \mathbf{u}: u_i \in H^1(\Omega); \mathbf{u} = \mathbf{0} \text{ on } \Gamma_u \right\}$.

3 Discrete formulation and solution algorithm

Equations (20a,b) comprise a mixed variational problem for the optimal solution $(\rho, \mathbf{u}) \in V_\rho \times V_u$ based on the first-order Kuhn-Tucker conditions. We now construct a mixed finite element method for solving this problem in the discrete space $V_{\rho h} \times V_{uh}$, where

$$V_{\rho h} = \left\{ \rho \in L_\infty(\Omega): \rho|_{\Omega_e^\alpha} \in H^1\left(\Omega_e^\alpha\right); \rho = \mathbf{N}_\rho \hat{\rho};\, 0 < \rho_{\min} \le \rho \le 1 \text{ in } \Omega \right\};$$

$$V_{uh} = \left\{ \mathbf{u}: u_i \in H^1(\Omega): \mathbf{u} = \mathbf{N}_u \hat{\mathbf{u}};\, \mathbf{u} = \bar{\mathbf{u}} \text{ on } \Gamma_u \right\} \text{ and}$$

$$V_{u0h} = \left\{ \mathbf{u}: u_i \in H^1(\Omega): \mathbf{u} = \mathbf{N}_u \hat{\mathbf{u}};\, \mathbf{u} = \mathbf{0} \text{ on } \Gamma_u \right\}. \tag{21}$$

$\mathbf{N}_\rho$ and $\mathbf{N}_u$ are matrices containing finite element basis functions for the interpolation parameter and displacement vector, Ω_e^α is the interior of element α, $\hat{\rho} \in \Re^{n_\rho}$ and $\hat{\mathbf{u}} \in \Re^{n_u}$. The disjoint regions Ω_α referenced in section 2 are identified with the individual finite element interiors Ω_e^α. $V_{\rho h}$ admits jumps across the interelement boundaries, which constitute the jump set Γ_J.

The discrete approximation of problem (17) is given by

$$\max_{\rho \in V_{\rho h}} \min_{\mathbf{u} \in V_{uh}} \Pi + \alpha S_1 + \beta S_2 - \lambda\left[V(\rho) - \bar{V} \right]. \tag{22}$$

The stationary conditions for problem (22) lead to the discrete, mixed variational problem:

Find $(\mathbf{u},\rho) \in V_{uh} \times V_{\rho h}$ such that

$$\int_\Omega \varepsilon(\mathbf{v}) : \frac{\partial W}{\partial \varepsilon} d\Omega = \int_\Omega \mathbf{v} \cdot \mathbf{b}\, d\Omega + \int_{\Gamma_t} \mathbf{v} \cdot \mathbf{t}\, d\Gamma \quad \forall \mathbf{v} \in V_{u0h} \quad \text{and} \tag{23a}$$

$$\int_\Omega q \left(\frac{\partial W}{\partial \rho} + \alpha \frac{df}{d\rho} \right) d\Omega + \beta \frac{dS_2}{dP} \left(\int_{\Omega \setminus \Gamma_J} \nabla q^T \left. \frac{\partial g_h}{\partial \mathbf{w}} \right|_{\mathbf{w}=\nabla\rho} d\Omega + \int_{\Gamma_J} \langle q \rangle \left. \frac{\partial j}{\partial r} \right|_{r=\langle\rho\rangle} d\Gamma \right) = \lambda \int_\Omega q\, d\Omega \quad \forall q \in V_{\rho h} \tag{23b}$$

Equation (23a) is the familiar stiffness equation. The optimality condition (23b) can be expressed as

$$\int_\Omega N_{\rho\gamma} \left(\frac{\partial W}{\partial \rho} + \alpha \frac{df}{d\rho} \right) d\Omega + \beta(1+2\xi) \frac{dS_2}{dP} \left\{ \int_{\Omega \setminus \Gamma_J} \frac{\nabla N_{\rho\gamma}^T \nabla \rho}{\left[(1+2\xi) \nabla\rho^T \nabla\rho + \frac{\xi^2}{h^2} \right]^{1/2}} d\Omega \right. \tag{24}$$

$$\left. + \int_{\Gamma_J} \frac{\langle N_{\rho\gamma} \rangle \langle \rho \rangle}{\left[(1+2\xi) \langle\rho\rangle^2 + \xi^2 \right]^{1/2}} d\Gamma \right\} = \lambda \int_\Omega N_{\rho\gamma}\, d\Omega; \quad \gamma = 1, n_\rho$$

in which $N_{\rho\gamma}$ is a discrete basis function for $V_{\rho h}$, and n_ρ is the dimension of $V_{\rho h}$. We note that the mixed variational form of the discrete problem (23) is significant. Care must be exercised in the selection of the discrete function spaces, V_{uh} and $V_{\rho h}$, to avoid "checkerboard" patterns and other grid-scale anomalies in the solution (Jog and Haber, 1995).

We employ a nested, iterative solution strategy to solve the discrete problem (23). Each outer iteration includes two steps: a stiffness analysis and a design update. The stiffness analysis determines a displacement solution that satisfies the equilibrium equation (23a) using the current design estimate. The design update is itself an iterative procedure that determines an estimate of (λ, ρ) that simultaneously satisfies the volume constraint and the optimality criterion (23b) using the estimate of the displacement solution from the previous stiffness analysis (see (Jog, Haber and Bendsøe, 1993 and 1994) for details). The penalty parameters α and β can be adjusted to improve numerical performance. In our implementation, α is held constant while β is reduced in each outer iteration i to improve the accuracy of the interior penalty method:

$$\beta^{i+1} = \varsigma\beta^i; \quad 0 < \varsigma \leq 1. \tag{25}$$

4 Numerical examples

The first example illustrates the mesh-dependent nature of designs obtained by penalized methods without perimeter control. Solutions for the bicycle wheel problem (see Fig. 2a) were computed on uniform grids with different levels of refinement. In these examples, the parameter α was gradually increased to penalize intermediate values of ρ and the parameter β was taken as zero. The coarse mesh (Fig. 7a) is able to represent relatively few spokes in the wheel design, while the fine mesh (Fig. 7b) is able to resolve a larger number of spokes. Additional grid refinement would generate increasingly complicated designs, since the compliance reduces as the number of spokes increases. Although the coarse discretization in Fig. 7a artificially reduces the computed compliance, we nonetheless observe a lower compliance for the design in Fig. 7b. On the other hand, this example illustrates a common finding: the reduction in compliance obtained by increasing the complexity of the design topology is relatively modest. Thus, effective designs can be obtained with relatively simple topologies. The perimeter method allows the designer to obtain good geometric resolution on a refined grid while restricting the search to simple topologies.

The remaining examples in this section present numerical results for the perimeter method based on the mixed variational problem (17). The interpolation parameter ρ is modelled as piecewise uniform per element and the displacement $\mathbf{u}$ is modelled by eight-node serendipity elements. The value of the smoothing parameter is $\xi = 0.5$. We use an iterative solution algorithm in which an optimality criterion method (Jog *et al.*, 1994) determines the incremental design updates. The parameter α is held constant, while β is decreased by a constant factor before each design iteration to reduce the error in the approximation of the perimeter constraint. β_0 and β_f denote the given starting and final values for β.

Table 1. Optimization parameters and results for the bicycle wheel design problem.

Fig.	grid size (half)	$\overline{V}/\|\Omega\|$	$\overline{P}(L)$	α	β_0	β_f	$J(\|F\|L)$	$P(L)$
8a	32 x 40	25%	21.5	80	30	0.5	.03583	20.5
8b	48 x 60	25%	21.5	80	20	0.5	.03620	20.5

Fig. 8 shows two solutions obtained with the proposed perimeter method for the bicycle wheel problem of Fig. 2a. The structural data are $E = 0.875 \times 10^4 |F| L^{-2}$, $\nu = 0.25$ and $t = 0.1L$. We invoked symmetry to reduce the problem size, using meshes of 32 x 40 elements and 48 x 60 elements to model one half the structure (all statistics cited in this and the following example pertain to one half of the symmetrical structure). The optimization parameters and results for the two cases are displayed in Table 1. This example demonstrates the improved geometric resolution that can be obtained with grid refinement in the perimeter method. This example required some tuning of the optimization parameters (note the distinct values of β_0 in this example) to ensure that the same local extremum was obtained on the two grids. Both solutions were obtained in 70 design iterations.

Table 2. Optimization parameters and results for the MBB design problem.

Fig.	grid size (half)	$\overline{V}/\|\Omega\|$	$\overline{P}(L)$	α	β_0	β_f	$J(\|F\|L)$	$P(L)$
9a	16 x 40	60%	--	0	0	0	.01198	∞
9b	32 x 80	60%	--	0	0	0	.01223	∞
9c	16 x 40	60%	--	150	0	0	.01253	21.2
9d	32 x 80	60%	--	150	0	0	.01282	29.0
10a	16 x 40	60%	30	150	2.0	0.1	.01258	21.9
10b	32 x 80	60%	30	150	2.0	0.1	.01285	26.5
10c	16 x 40	60%	24	150	4.0	0.1	.01266	21.8
10d	32 x 80	60%	24	150	4.0	0.1	.01300	22.6
10e	16 x 40	60%	22	150	5.0	0.1	.01287	18.7
10f	32 x 80	60%	22	150	5.0	0.1	.01312	20.5
10g	16 x 40	60%	18	150	5.0	0.6	.01317	15.6

The next example involves the design of a simply-supported aircraft floor beam a carrying a midspan point load, as illustrated in Fig. 2b (this problem is sometimes called the *MBB beam problem* in the topology design literature). The outer frame of the beam is constrained to be solid, while material in the inner region may be distributed freely to obtain a 60% volume fraction overall. The structural data are $E = 0.875 \times 10^2 |F| L^{-2}$, $\nu = 0.25$ and $t = 1.0L$. Optimization parameters and numerical results for the cases described below are listed in Table 2; all solutions were obtained in 50 design iterations and symmetry was invoked to limit the model to half of the structure.

Fig. 9 shows designs that were obtained without perimeter control. The solution in Figs. 9a and 9b are solutions to the unpenalized, relaxed problem obtained on a relatively coarse grid (16 x 40) and a refined grid (32 x 80) using the analytically optimal rank-2 microstructure described in (Jog, Haber and Bendsøe, 1994). The density distribution contains extensive regions of "grey" perforated material, as is expected in a relaxed solution. Note that the smooth density distribution yields a very low perimeter measure, according to the definition in equation (14). However, the true perimeter is infinite if one considers the microscopic perforations in the rank-2 model. Although these designs would be difficult to fabricate, they do provide approximate lower-bounds on the compliance. Fig. 9c shows the coarse-grid design obtained by adding a penalty on intermediate density ($\alpha = 150$). The amount of gray material is reduced, and the suggestion of a macroscopic topology is evident. The compliance of the penalized design is higher than that of the unpenalized rank-2 solution, as expected. In this case, the relatively coarse mesh controls the complexity of the design. The same problem parameters generate a different design topology when applied to the refined grid in Fig. 9d. In the absence of perimeter control, the mesh resolution controls the design complexity, so we do not obtain a mesh-independent optimal design topology.

Fig. 10 illustrates the use of the perimeter method to control the optimal topology and to achieve mesh-independent solutions. The results in Figs. 10a and 10b are based on a perimeter bound $\overline{P} = 30L$. While the coarse grid in Fig. 10a is not able to completely resolve the design, the optimal topology is essentially the same as the one obtained with the refined grid in Fig. 10b. The characteristic Michel-truss layout is evident. A simpler optimal topology is obtained by reducing the perimeter bound to $\overline{P} = 24L$. The same optimal topology is clearly evident in Figs. 10c and 10d, demonstrating the ability of the perimeter method to generate mesh-independent solutions. An even simpler design is obtained by further reducing the perimeter bound to $\overline{P} = 22L$ in Figs 10e and 10f. The solutions on refined grids (e.g., Figs. 10b and 10d) reveal significant design details, such as the fillets between intersecting members that prevent stress concentrations. This ability

to resolve geometric detail extends the applicability of the perimeter method beyond preliminary design; there is no need to resort to fixed-topology shape optimization procedures to obtain a final design. Fig. 10g shows a very simple topology obtained by setting $\overline{P} = 18L$.

One cannot directly compare the compliance values (J) obtained on different numerical grids, because the discretization error associated with a coarser mesh artificially reduces the compliance. However, the trade-off between stiffness (low compliance) and perimeter is clearly evident when we compare designs obtained on the same grid (Figs. 10a, 10c, 10e and 10g for the coarse grid and Figs. 10b, 10d and 10f for the refined grid). Improved stiffness can be achieved at the cost of design complexity; the compliance increases as we decrease the perimeter bound to achieve a simpler design. On the other hand, the results show that designs with simple, practical topologies can be achieved with a relatively small increase in compliance.

5 Conclusions

The perimeter method is an attractive alternative for variable-topology shape optimization problems. Placing a bound on the design perimeter restricts the feasible design space to eliminate chattering solutions and thereby ensures a well-posed problem. At the same time, the complexities of microstructure and homogenization methods are circumvented. As a result, the method is not restricted to compliance optimization -- it is evidently extensible to general classes of objectives and constraints and there are no intrinsic difficulties in extensions to three dimensions.

The ability to control the complexity of the solution -- i.e., the number and scale of holes in the optimal design -- is one of the key advantages of the perimeter method. Because the perimeter bound (rather than element size) controls the complexity of the design, improved geometric resolution can be achieved via mesh refinement. Thus, a designer can generate practical, manufacturable designs in a single automatic operation to any desired level of precision. There is no need to post-process the solution with image processing, manual CAD methods, or fixed-topology shape optimization procedures. Adaptive analysis methods could be used to concentrate elements where either the mechanical response or the optimal design geometry demands improved resolution.

The essence of the perimeter method is formulated in the integer problem (12); the subsequent development in this paper represents but one way to implement the concept numerically. In principal, one could develop a direct integer solution method for (12). However, the large-scale optimization problems and the expensive function evaluations

encountered in topology design preclude this approach for practical problems. A solution algorithm based on a continuous approximation to the integer problem appears to be a practical necessity. The continuous approximation and solution algorithm described above represent only one possibility; it would be worthwhile to explore alternatives. For example, one could use math programming methods to solve the optimization problem in lieu of the optimiality criterion method; the inequality constraint on the perimeter could be enforced by the optimization algorithm, rather than by an interior penalty method. Within the framework of the continuous problem (17), one could explore alternative definitions of the penalty functions S_1 and S_2 and of the smoothed perimeter measure given by (14).

The perimeter method ensures the existence of an optimal solution, but it does not address uniqueness -- there may be many local extrema. Thus, the mesh independence observed in numerical solutions based on the perimeter method is a local property that only holds in the neighborhood of a local extremum of the continuum problem (17). The perimeter constraint provides some relief because it precludes local extrema with high perimeter measures. However, there might still be undesirable solutions among the multiple extrema that do satisfy the perimeter constraint. Therefore, one must take steps to prevent the solution algorithm from converging to an undesirable local extremum and to increase the likelihood that it will find the same optimal design on different grids. In the present work, we attempt to minimize the negative effects of the penalty term by using the smallest value of the parameter α that is consistent with a good approximation to the integer design problem. This allows the potential energy term in the design functional to guide the solution to a favorable design. While α was constant in the examples reported here, it might be beneficial to gradually increase α over a number of design iterations, starting from a small initial value. As in any penalty method, some tuning is required to obtain good schedules for α and β.

It should be noted that the problems associated with multiple local extrema are not peculiar to the perimeter method; they are intrinsic to penalized topology design formulations. Although the relaxation in the unpenalized homogenization method eliminates most (if not all) local extrema, this favorable property does not carry over to penalized homogenization methods (which may even be ill-posed unless the solution space is properly restricted). The development of a practical optimization technique that effectively addresses the problem of multiple local extrema is a worthy goal for continuing research in topology design.

The raster geometry model (uniform ρ within each finite element) makes the perimeter measure dependent on mesh orientation. The perimeter of an edge segment that parallels one of the principal directions of a square grid is computed exactly, while the

perimeter of a segment oriented at 45 degrees is overestimated by a factor of $\sqrt{2}$. Although this artificially favors edges that are parallel to the grid directions, the orientation-dependence does not appear to have significantly influenced our optimal designs. The orientation dependence could be reduced or eliminated by using either a non-uniform interpolation for ρ within each element or a non-local sampling algorithm, as described by Sigmund (1995).

Acknowledgements

The authors wish to acknowledge the following organizations for their support. The National Science Foundation (U.S.A.), the Danish Research Academy, the Danish Technical Research Council (Program for Research on Computer-Aided Design) and the Center for Supercomputing Research & Development. Computations were performed on the Silicon Graphics Power Challenge System at the National Center for Supercomputing Applications.

References

Allaire, G.; Francfort, G. A. 1993: A numerical algorithm for topology and shape optimization," In: Bendsøe, M. P.; Moto Soares, C. A. (eds.) *Topology design of structures*, pp. 239-248. Dordrecht: Kluwer

Allaire, G.; Kohn, R. V. 1993: Topology design and optimal shape design using homogenization. In: Bendsøe, M. P.; Moto Soares, C. A. (eds.) *Topology design of structures*, pp. 207-218. Dordrecht: Kluwer

Ambrosio, L.; and Buttazzo, G. 1993: An optimal design problem with perimeter penalization. *Calculus of Variations and Partial Differential Equations* **1**, 55-69

Bendsøe, M. P. 1989: Optimal shape design as a material distribution problem. *Struct. Optim.* **1**, 193-202

Bendsøe, M. P.; Diaz, A.; Kikuchi, N. 1993: Topology and generalized layout optimization of elastic structures. In: Bendsøe, M. P.; Moto Soares, C. A. (eds.) *Topology design of structures*, pp. 159-205. Dordrecht: Kluwer

Bendsøe, M. P.; Kikuchi, N. 1988: Generating optimal topologies in structural design using a homogenization method. *Computer Methods in Applied Mechanics and Engineering* **71**, 197-224

Cheng, K. T.; Olhoff, N. 1981: An investigation concerning optimal design of solid elastic plates. *International Journal of Solids and Structures* **17**, 305-323

Eschenauer, H. A.; Kobolev, V.; Schumacher, A. 1994: Bubble method of topology and shape optimization of structures. *Struct. Optim.* **8**, 42-51

Evans, L. C.; Gariepy, R. F. 1992: *Measure theory and fine properties of functions*, Boca Ratan: CRC Press

Gibianski, L. V.; Cherkaev, A. V. 1987: Microstructures of composites of extremal rigidity and exact estimates of the associated energy density. Ioffe Physicotechnical Institute preprint 1115, Leningrad (in Russian); also in: Kohn, R. V. (ed.) *Topics in the Mathematical Modeling of Composite Materials,* Birkhauser, New York, 1994.

Goodman, J.; Kohn, R. V.; Reyna, L. 1986: Numerical study of a relaxed variational problem for optimal design. *Computer Methods in Applied Mechanics and Engineering* **57**, 107-127

Haber, R. B.; Jog, C. S.; Bendsøe, M. P. 1994: Variable-topology shape optimization with a control on perimeter. In: Gilmore, B. J., Hoeltzel, D. A., Dutta, D., Eschenauer, H. A. (eds.) *Advances in Design Automation*, ASME DE-Vol. 69-2, pp 261-272.

Jog, C. S.; Haber, R. B.; Bendsøe, M. P. 1993: A displacement-based topology design method with self-adaptive layered materials. In: Bendsøe, M. P.; Moto Soares, C. A. (eds.) *Topology design of structures*, pp. 219-238. Dordrecht: Kluwer

Jog, C. S.; Haber, R. B.; Bendsøe, M. P. 1994: Topology design with optimized, self-adaptive materials. *Int. J. Num. Methods Engng.* **37**, 1323-1350

Jog, C. S.; Haber, R. B. 1995: Stability of Finite Element Models for Distributed-Parameter Optimization and Topology Design. *Computer Methods in Applied Mechanics and Engineering* (to appear)

Kohn, R. V. 1991: Composite materials and structural optimization," *Proc. Workshop on Smart/Intelligent Materials and Systems*, Honolulu, March 1990. Technomic Press, Lancaster, Pa., USA

Kohn, R. V.; Strang, G. 1986: Optimal design and relaxation of variational problems. *Communications in Pure and Applied Mathematics* **39**, 1-25 (part I), 139-182 (part II), 353-377 (Part III)

Lurie, A. K.; Federov, A. V.; Cherkaev, A. V. 1982: Regularization of optimal design problems for bars and plates. *Journal of Optimization Theory and Applications* **37**, 499-521 (part I), 523-543 (part II)

Mlejnek, H. 1992: Some aspects of the genesis of structures, *Struct. Optim.*. **5**, 64-69.

Murat, F. 1977: Contre-exemples pour divers problemes ou le controle intervient dans les coefficients. *Ann. Mat. Pura et Appl.* **112**, 49-68

Murat, F.; Tartar, L. 1985: Calcul des variations et homogeneisation. *Les Methodes de l'Homogeneisation: Theorie et Applications en Physique*, pp. 319-370, Coll. de la Dir. des Etudes et Recherches de Electricite de France, Eyrolles, Paris

Rodrigues, H.; Fernandes, P. 1995: A material based model for topology optimization of thermoelastic structures. *Int. J. Num. Methods Engng.* **38**, 1951-1965

Rozvany, G.I.N. 1993: Layout theory for grid-type structures. In: Bendsøe, M. P.; Moto Soares, C. A. (eds.) *Topology design of structures*, pp. 251-272. Dordrecht: Kluwer

Sigmund, O. 1995: Design of material structures using topology optimization. DCAMM Special Report no. S69, Technical University of Denmark.

Sokolnikoff, I. S. 1987: *Mathematical Theory of Elasticity*, Florida: Robert Krieger

Suzuki, K.; Kikuchi, N. 1991: Shape and topology optimization for generalized layout problems using the homogenization method. *Comp. Meth. Appl. Mechs. Engng.* **93**, 291-318

Tartar, L. 1977: Estimation de coefficents homogeneises. *Lecture Notes in Mathematics* **704**, pp. 364-373. Berlin: Springer Verlag

Wheedon, R. L.; Zygmund, A. 1977: *Measure and integral: an introduction to real analysis*, Monographs in Pure and Applied Math. **43**, New York: Marcel Dekker

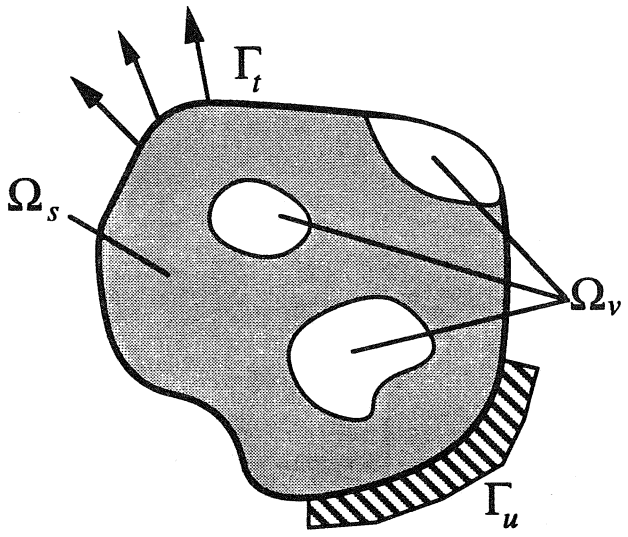

Fig. 1. Domain diagram for the variable-topology optimization problem

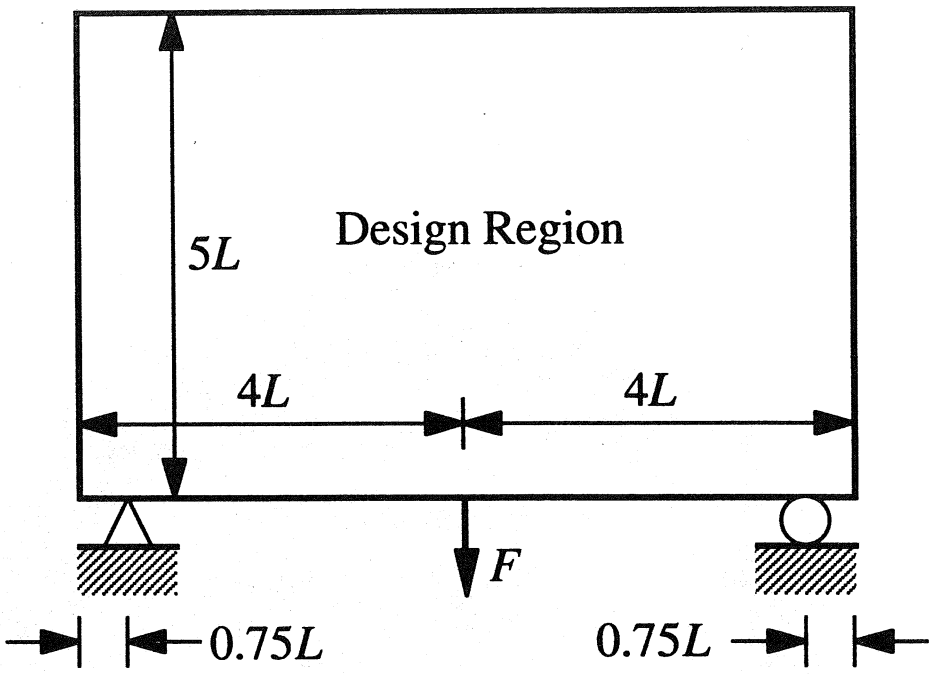

(a)

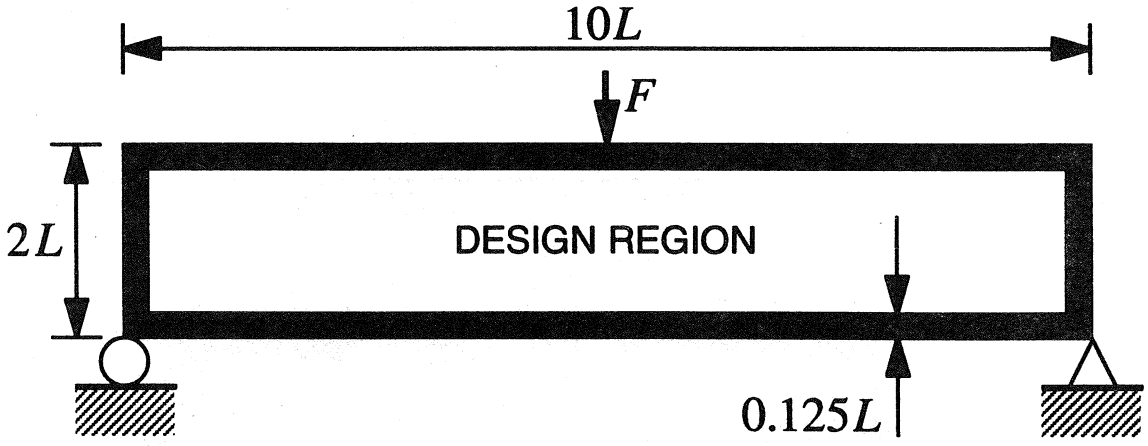

(b)

Fig. 2. Design domains, loadings and support conditions for example problems: (a) bicycle wheel problem; (b) MBB beam problem

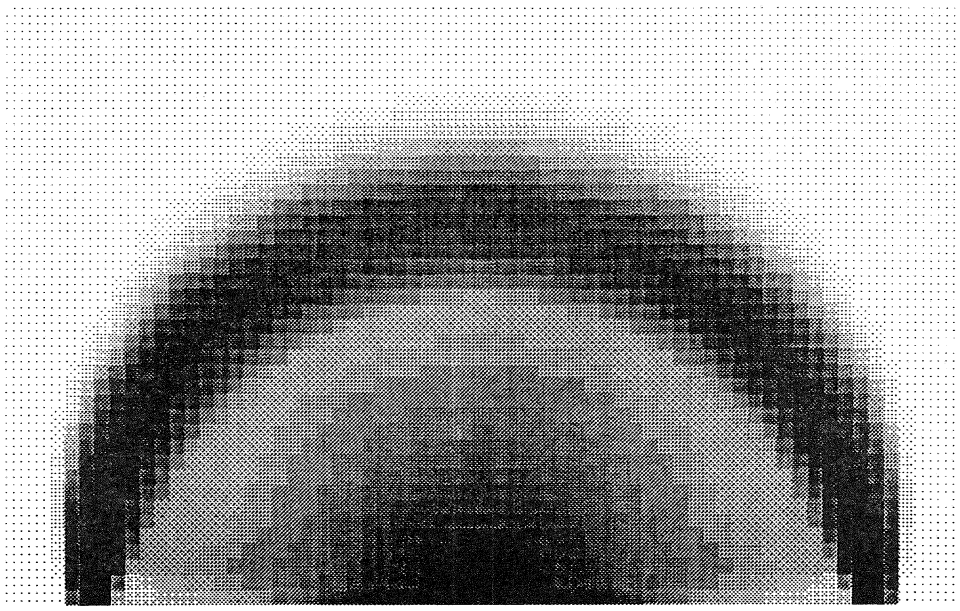

Fig. 3. Optimal bulk density distribution for the relaxed bicycle wheel problem

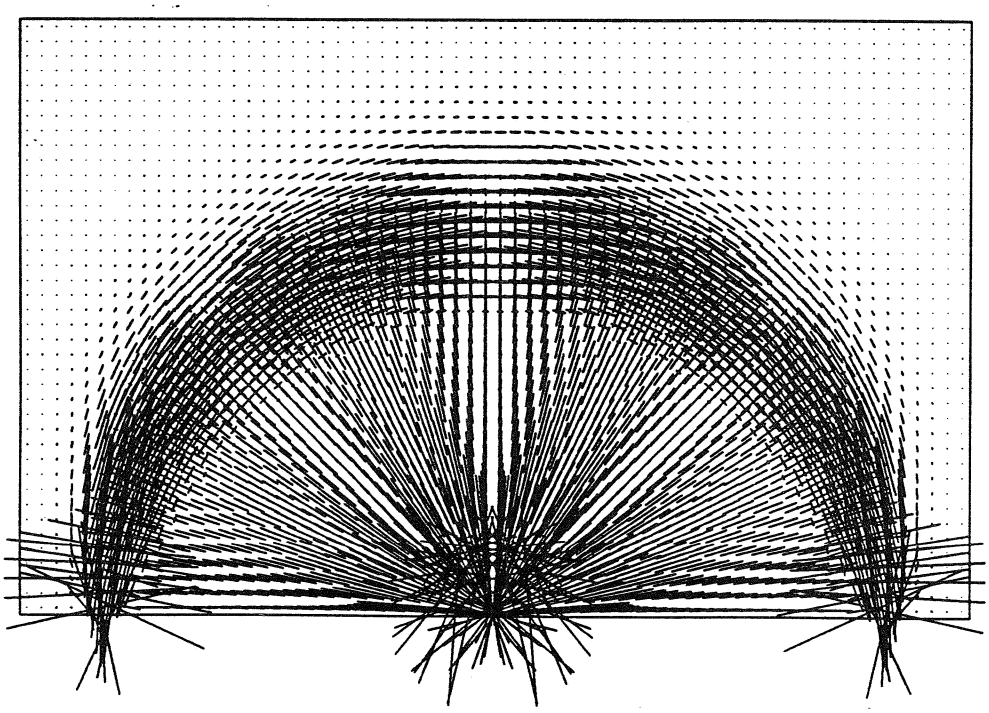

Fig. 4. Optimal microstructure configuration for the relaxed bicycle wheel problem

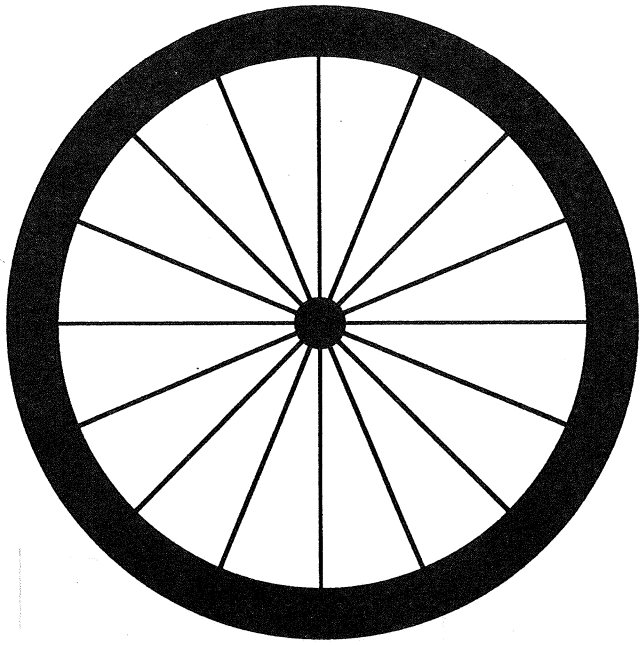

(a)

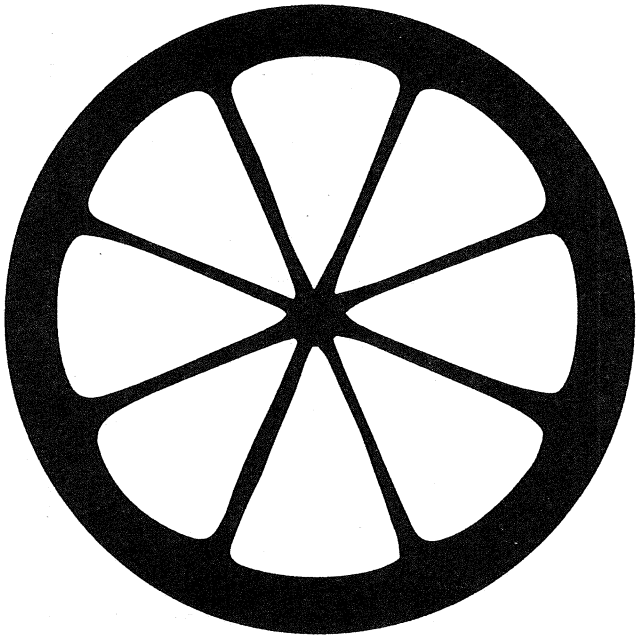

(b)

Fig. 5. Practical realizations of the relaxed solution for the bicycle wheel problem
(a) hub, rim and wire spokes; (b) solid disk with cut-out holes

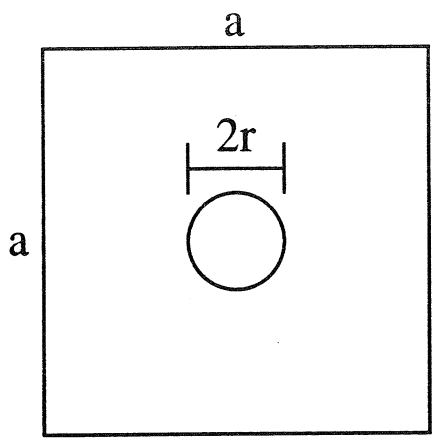

(a)

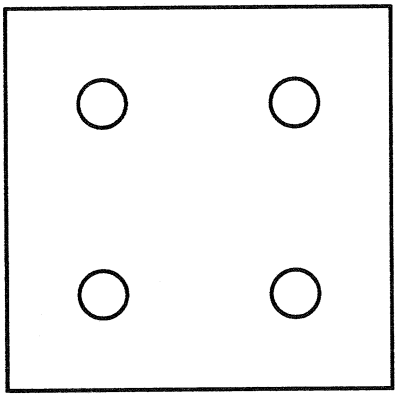

(b)

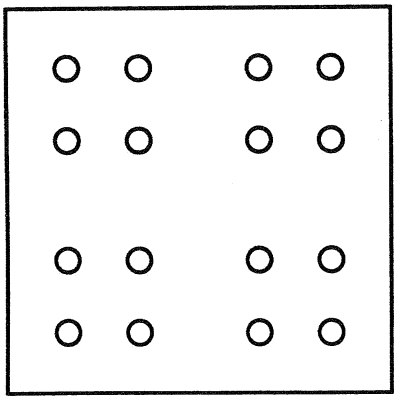

(c)

Fig. 6. Relation between hole radius r and perimeter P in a plate with uniform thickness t and volume, $\overline{V} = (a^2 - 4\pi)t$: (a) $r = 2, P = 4\pi$; (b) $r = 1, P = 8\pi$; (c) $r = 0.5, P = 16\pi$

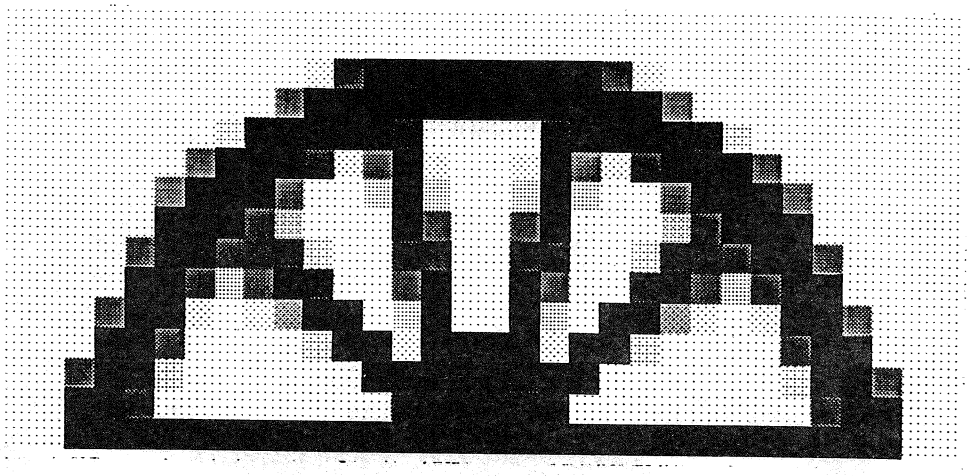

(a)

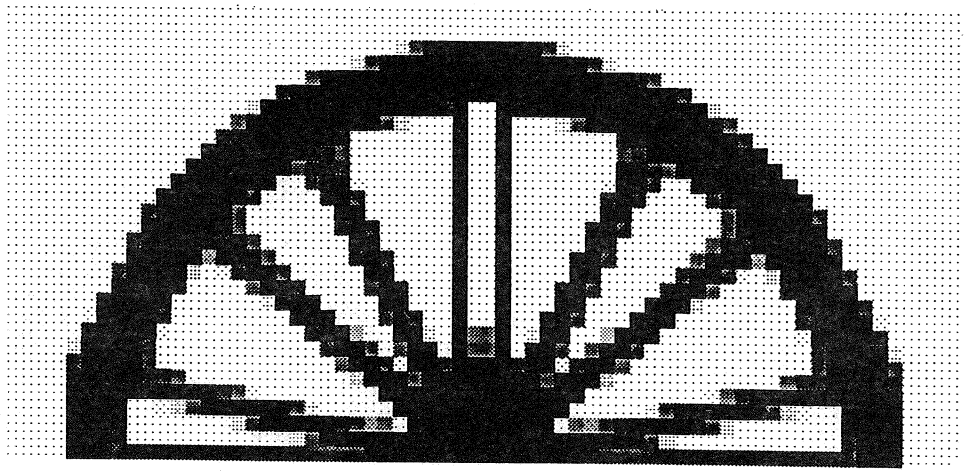

(b)

Fig. 7. Optimal designs for the penalized bicycle wheel problem without perimeter control: (a) 16 x 20 elements; (b) 32 x 40 elements

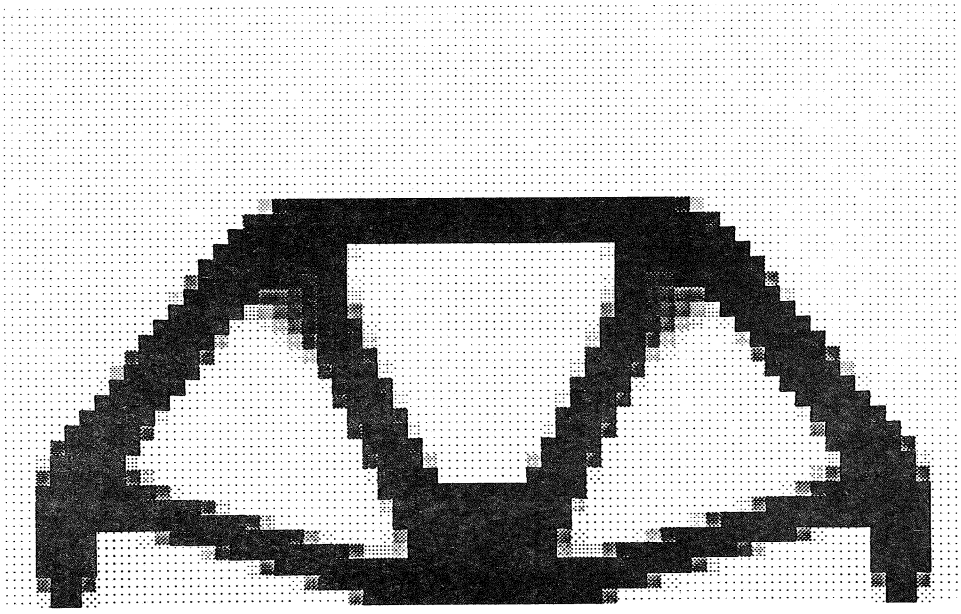

(a)

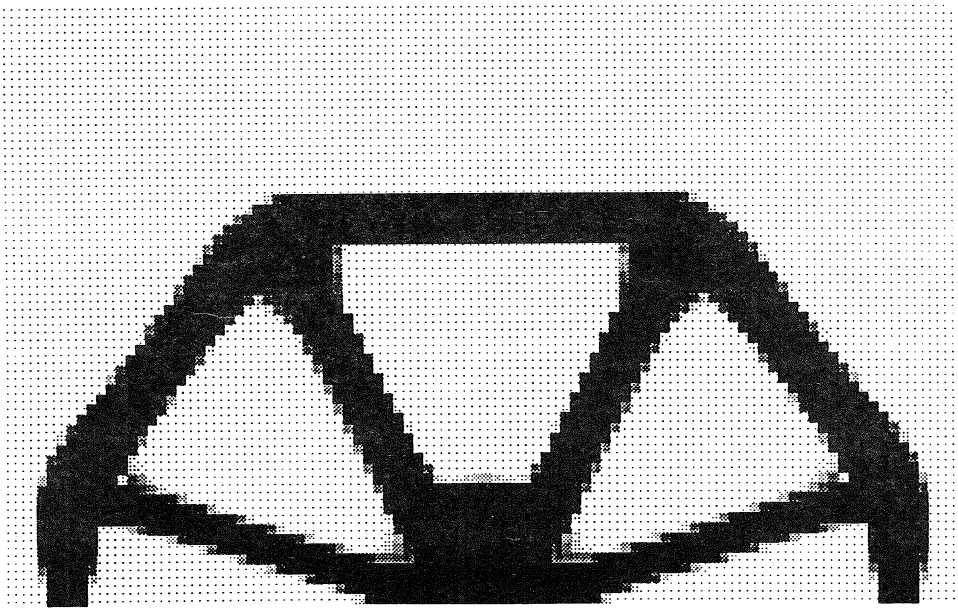

(b)

Fig. 8. Optimal designs for the penalized bicycle wheel problem with perimeter control: (a) 32 x 40 elements; (b) 48 x 60 elements

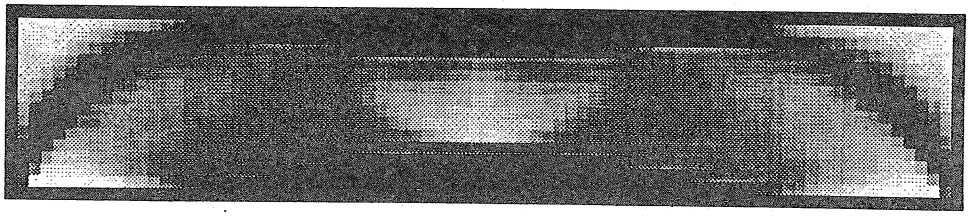

(a)

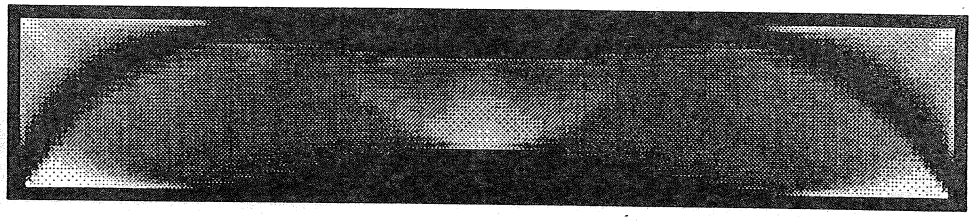

(b)

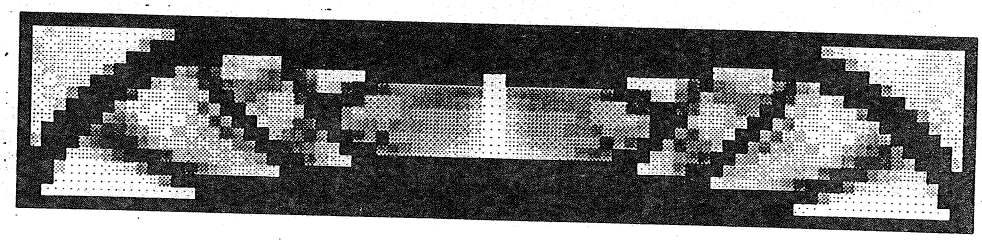

(c)

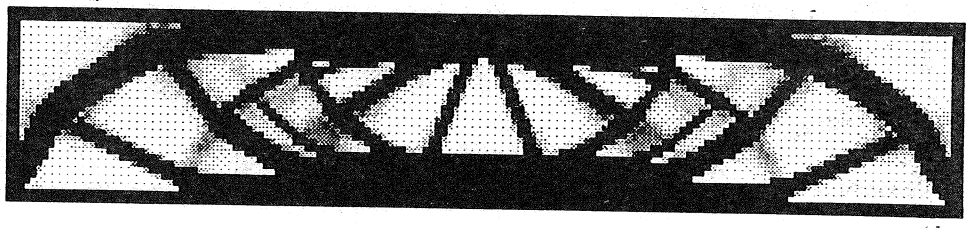

(d)

Fig. 9. Solutions for the MBB beam problem without perimeter control:
(a) relaxed solution, coarse grid; (b) relaxed solution, fine grid; (c) penalized solution, coarse grid; (d) penalized solution, fine grid

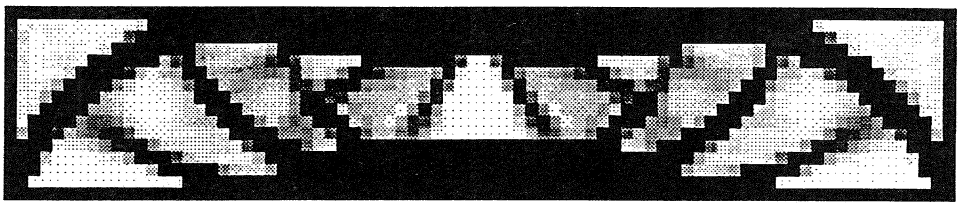

(a)

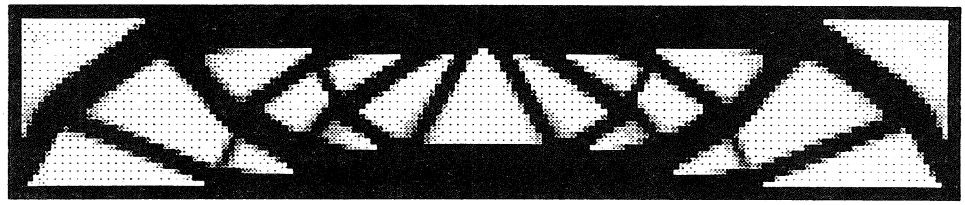

(b)

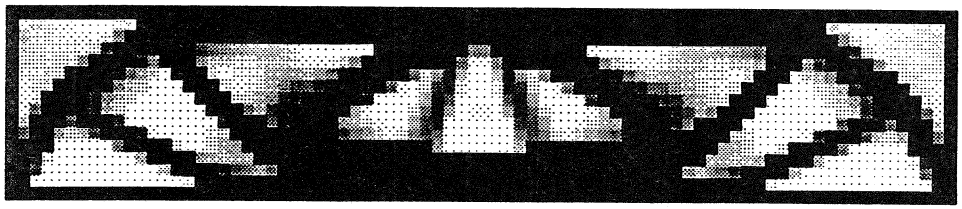

(c)

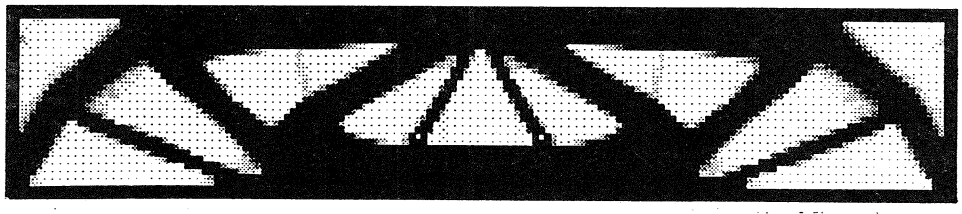

(d)

Fig. 10. Solutions for the MBB beam problem with perimeter control:
(a) $\overline{P} = 30L$, coarse grid; (b) $\overline{P} = 30L$, fine grid;
(c) $\overline{P} = 24L$, coarse grid; (d) $\overline{P} = 24L$, fine grid

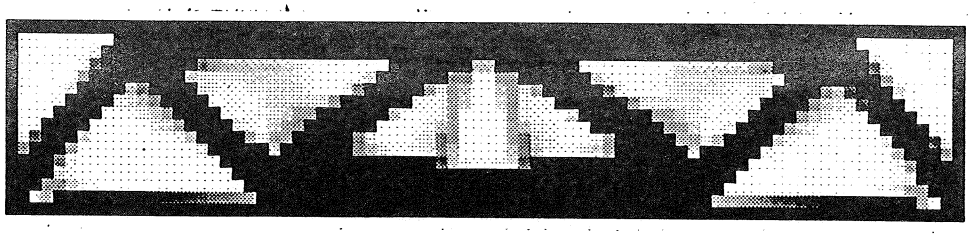

(e)

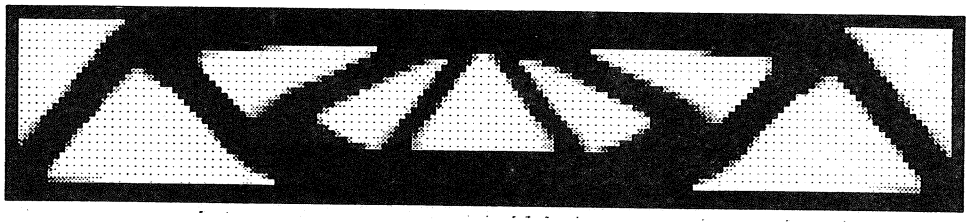

(f)

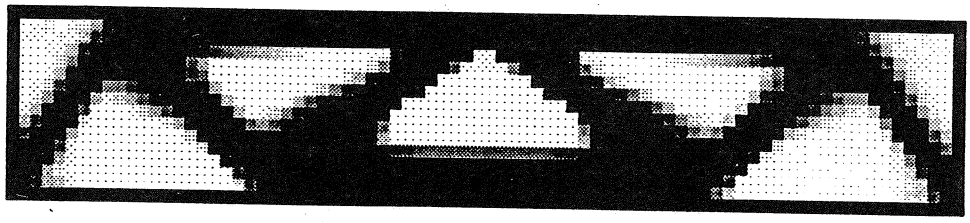

(g)

Fig. 10 (cont.). Solutions for the MBB beam problem with perimeter control: (e) $\overline{P} = 22L$, coarse grid; (f) $\overline{P} = 22L$, fine grid; (g) $\overline{P} = 18L$, coarse grid

List of Recent TAM Reports

No.	Authors	Title	Date
735	Mei, R., R. J. Adrian, and T. J. Hanratty	Particle dispersion in isotropic turbulence under the influence of non-Stokesian drag and gravitational settling	Nov. 1993
736	Dey, N., D. F. Socie, and K. J. Hsia	Static and cyclic fatigue failure at high temperature in ceramics containing grain boundary viscous phase, Part I: Experiments	Nov. 1993
737	Dey, N., D. F. Socie, and K. J. Hsia	Static and cyclic fatigue failure at high temperature in ceramics containing grain boundary viscous phase, Part II: Modeling—*Acta Metallurgica et Materialia*, **43**, 2163-2175 (1995)	Nov. 1993
738	Turner, J. A., and R. L. Weaver	Radiative transfer and multiple scattering of diffuse ultrasound in polycrystalline media—*Journal of the Acoustical Society of America* **96**, 3675–3681 (1994)	Nov. 1993
739	Qi, Q., and R. E. Johnson	Resin flows through a porous fiber collection in pultrusion processing	Dec. 1993
740	Weaver, R. L., W. Sachse, and K. Y. Kim	Transient elastic waves in a transversely isotropic plate—*Journal of Applied Mechanics*, in press (1996)	Dec. 1993
741	Zhang, Y., and R. L. Weaver	Scattering from a thin random fluid layer—*Journal of the Acoustical Society of America* **96**, 1899–1909 (1994)	Dec. 1993
742	Weaver, R. L., and W. Sachse	Diffusion of ultrasound in a glass bead slurry—*Journal of the Acoustical Society of America* **97**, 2094–2102 (1995)	Dec. 1993
743	Sundermeyer, J. N., and R. L. Weaver	On crack identification and characterization in a beam by nonlinear vibration analysis—*Journal of Sound and Vibration* **183**, 857–872 (1995)	Dec. 1993
744	Li, L., and N. R. Sottos	Predictions of static displacements in 1–3 piezocomposites—*Journal of Intelligent Materials Systems and Structures* **6**, 169–180 (1995)	Dec. 1993
745	Jones, S. W.	Chaotic advection and dispersion—*Physica D* **76**, 55–69 (1994)	Jan. 1994
746	Stewart, D. S., and J. Yao	Critical detonation shock curvature and failure dynamics: Developments in the theory of detonation shock dynamics—*Developments in Theoretical and Applied Mechanics* **17** (1994)	Feb. 1994
747	Mei, R., and R. J. Adrian	Effect of Reynolds-number-dependent turbulence structure on the dispersion of fluid and particles—*Journal of Fluids Engineering*, **117**, 402-409 (1995)	Feb. 1994
748	Liu, Z.-C., R. J. Adrian, and T. J. Hanratty	Reynolds-number similarity of orthogonal decomposition of the outer layer of turbulent wall flow—*Physics of Fluids* **6**, 2815–2819 (1994)	Feb. 1994
749	Barnhart, D. H., R. J. Adrian, and G. C. Papen	Phase-conjugate holographic system for high-resolution particle image velocimetry—*Applied Optics* **33**, 7159–7170 (1994)	Feb. 1994
750	Qi, Q., W. D. O'Brien Jr., and J. G. Harris	The propagation of ultrasonic waves through a bubbly liquid into tissue: A linear analysis—*IEEE Transactions on Ultrasonics, Ferroelectrics and Frequency Control* **42**, 28–36 (1995)	Mar. 1994
751	Mittal, R., and S. Balachandar	Direct numerical simulation of flow past elliptic cylinders—*Journal of Computational Mechanics*, in press (1996)	May 1994
752	Students in TAM 293–294	Thirty-first student symposium on engineering mechanics, J. W. Phillips, coordinator: Selected senior projects by D. N. Anderson, J. R. Dahlen, M. J. Danyluk, A. M. Dreyer, K. M. Durkin, J. J. Kriegsmann, J. T. McGonigle, and V. Tyagi	May 1994
753	Thoroddsen, S. T.	The failure of the Kolmogorov refined similarity hypothesis in fluid turbulence—*Physics of Fluids* **7**, 691–693 (1995)	May 1994
754	Turner, J. A., and R. L. Weaver	Time dependence of multiply scattered diffuse ultrasound in polycrystalline media—*Journal of the Acoustical Society of America* **97**, 2639–2644 (1995)	June 1994

List of Recent TAM Reports (cont'd)

No.	Authors	Title	Date
755	Riahi, D. N.	Finite-amplitude thermal convection with spatially modulated boundary temperatures—*Proceedings of the Royal Society of London A* **449**, 459–478 (1995)	June 1994
756	Riahi, D. N.	Renormalization group analysis for stratified turbulence—*International Journal of Mathematics and Mathematical Sciences*, in press (1996)	June 1994
757	Riahi, D. N.	Wave-packet convection in a porous layer with boundary imperfections—*Journal of Fluid Mechanics*, in press (1996)	June 1994
758	Jog, C. S., and R. B. Haber	Stability of finite element models for distributed-parameter optimization and topology design—*Computer Methods in Applied Mechanics and Engineering*, in press (1996).	July 1994
759	Qi, Q., and G. J. Brereton	Mechanisms of removal of micron-sized particles by high-frequency ultrasonic waves—*IEEE Transactions on Ultrasonics, Ferroelectrics and Frequency Control* **42**, 619–629 (1995)	July 1994
760	Shawki, T. G.	On shear flow localization with traction-controlled boundaries—*International Journal of Solids and Structures* **32**, 2751–2778 (1995)	July 1994
761	Balachandar, S., D. A. Yuen, and D. M. Reuteler	High Rayleigh number convection at infinite Prandtl number with temperature-dependent viscosity	July 1994
762	Phillips, J. W.	Arthur Newell Talbot—Proceedings of a conference to honor TAM's first department head and his family	Aug. 1994
763	Man., C. S., and D. E. Carlson	On the traction problem of dead loading in linear elasticity with initial stress—*Archive for Rational Mechanics and Analysis* **128**, 223–247 (1994)	Aug. 1994
764	Zhang, Y., and R. L. Weaver	Leaky Rayleigh wave scattering from elastic media with random microstructures	Aug. 1994
765	Cortese, T. A., and S. Balachandar	High-performance spectral simulation of turbulent flows in massively parallel machines with distributed memory—*International Journal of Supercomputer Applications* **9**, 185–202 (1995)	Aug. 1994
766	Balachandar, S.	Signature of the transition zone in the tomographic results extracted through the eigenfunctions of the two-point correlation—*Geophysical Research Letters* **22**, 1941–1944 (1995)	Sept. 1994
767	Piomelli, U.	Large-eddy simulation of turbulent flows	Sept. 1994
768	Harris, J. G., D. A. Rebinsky, and G. R. Wickham	An integrated model of scattering from an imperfect interface—*Journal of the Acoustical Society of America*, in press (1996)	Sept. 1994
769	Hsia, K. J., and Z. Xu	The mathematical framework and an approximate solution of surface crack propagation under hydraulic pressure loading	Sept. 1994
770	Balachandar, S.	Two-point correlation and its eigen-decomposition for optimal characterization of mantle convection	Oct. 1994
771	Lufrano, J. M., and P. Sofronis	Numerical analysis of the interaction of solute hydrogen atoms with the stress field of a crack—*International Journal of Solids and Structures*, in press (1996)	Oct. 1994
772	Aref, H., and S. W. Jones	Motion of a solid body through ideal fluid	Oct. 1994
773	Stewart, D. S., T. D. Aslam, J. Yao, and J. B. Bdzil	Level-set techniques applied to unsteady detonation propagation—In "Modeling in Combustion Science," *Lecture Notes in Physics* (1995)	Oct. 1994
774	Mittal, R., and S. Balachandar	Effect of three-dimensionality on the lift and drag of circular and elliptic cylinders—*Physics of Fluids* **7**, 1841–1865 (1995)	Oct. 1994

List of Recent TAM Reports (cont'd)

No.	Authors	Title	Date
775	Stewart, D. S., T. D. Aslam, and J. Yao	On the evolution of cellular detonation	Nov. 1994 *Revised* Jan. 1996
776	Aref, H.	On the equilibrium and stability of a row of point vortices—*Journal of Fluid Mechanics* **290**, 167–181 (1995)	Nov. 1994
777	Cherukuri, H. P., T. G. Shawki, and M. El-Raheb	An accurate finite-difference scheme for elastic wave propagation in a circular disk—*Journal of the Acoustical Society of America,* in press (1996)	Nov. 1994
778	Li, L., and N. R. Sottos	Improving hydrostatic performance of 1–3 piezocomposites—*Journal of Applied Physics* **77**, 4595–4603 (1995)	Dec. 1994
779	Phillips, J. W., D. L. de Camara, M. D. Lockwood, and W. C. C. Grebner	Strength of silicone breast implants—*Plastic and Reconstructive Surgery* **97**, in press (1996)	Jan. 1995
780	Xin, Y.-B., K. J. Hsia, and D. A. Lange	Quantitative characterization of the fracture surface of silicon single crystals by confocal microscopy—*Journal of the American Ceramics Society* **78**, 3201-3208 (1995)	Jan. 1995
781	Yao, J., and D. S. Stewart	On the dynamics of multi-dimensional detonation—*Journal of Fluid Mechanics*, **309**, 225-275 (1996)	Jan. 1995
782	Riahi, D. N., and T. L. Sayre	Effect of rotation on the structure of a convecting mushy layer—*Acta Mechanica,* in press (1996)	Feb. 1995
783	Batchelor, G. K., and TAM faculty and students	A conversation with Professor George K. Batchelor	Feb. 1995
784	Sayre, T. L., and D. N. Riahi	Effect of rotation on flow instabilities during solidification of a binary alloy	Feb. 1995
785	Xin, Y.-B., and K. J. Hsia	A technique to generate straight surface cracks for studying the dislocation nucleation condition in brittle materials —*Acta Metallurgica et Materialia* **44**, 845-853 (1996).	Mar. 1995
786	Riahi, D. N.	Finite bandwidth, long wavelength convection with boundary imperfections: Near-resonant wavelength excitation	Mar. 1995
787	Turner, J. A., and R. L. Weaver	Average response of an infinite plate on a random foundation—*Journal of the Acoustical Society of America* **99**, in press (1996)	Mar. 1995
788	Weaver, R. L., and D. Sornette	The range of spectral correlations in pseudointegrable systems: GOE statistics in a rectangular membrane with a point scatterer—*Physical Review E*, **52**, 341 (1995)	April 1995
789	Students in TAM 293–294	Thirty-second student symposium on engineering mechanics, J. W. Phillips, coordinator: Selected senior projects by K. F. Anderson, M. B. Bishop, B. C. Case, S. R. McFarlin, J. M. Nowakowski, D. W. Peterson, C. V. Robertson, and C. E. Tsoukatos	April 1995
790	Figa, J., and C. J. Lawrence	Linear stability analysis of a gravity-driven Newtonian coating flow on a planar incline	May 1995
791	Figa, J., and C. J. Lawrence	Linear stability analysis of a gravity-driven viscosity-stratified Newtonian coating flow on a planar incline	May 1995
792	Cherukuri, H. P., and T. G. Shawki	On shear band nucleation and the finite propagation speed of thermal disturbances—*International Journal of Solids and Structures,* in press (1996)	May 1995
793	Harris, J. G.	Modeling scanned acoustic imaging of defects at solid interfaces—Chapter in *IMA Workshop on Inverse Problems in Wave Propagation,* Springer-Verlag, to appear (1996)	May 1995

List of Recent TAM Reports (cont'd)

No.	Authors	Title	Date
794	Sottos, N. R., J. M. Ockers, and M. J. Swindeman	Thermoelastic properties of plain weave composites for multilayer circuit board applications	May 1995
795	Aref, H., and M. A. Stremler	On the motion of three point vortices in a periodic strip—*Journal of Fluid Mechanics*, in press (1996).	June 1995
796	Barenblatt, G. I., and N. Goldenfeld	Does fully-developed turbulence exist? Reynolds number independence versus asymptotic covariance—*Physics of Fluids* **7**, 3078–3082 (1995)	June 1995
797	Aslam, T. D., J. B. Bdzil, and D. S. Stewart	Level set methods applied to modeling detonation shock dynamics—*Journal of Computational Physics*, in press (1996)	June 1995
798	Nimmagadda, P. B. R., and P. Sofronis	The effect of interface slip and diffusion on the creep strength of fiber and particulate composite materials—*Mechanics of Materials*, in press (1996)	July 1995
799	Hsia, K. J., T.-L. Zhang, and D. F. Socie	Effect of crack surface morphology on the fracture behavior under mixed mode loading —*ASTM Special Technical Publications*, STP 1296, in press (1996)	July 1995
800	Adrian, R. J.	Stochastic estimation of the structure of turbulent fields	Aug. 1995
801	Riahi, D. N.	Perturbation analysis and modeling for stratified turbulence	Aug. 1995
802	Thoroddsen, S. T.	Conditional sampling of dissipation in high Reynolds number turbulence —*Physics of Fluids*, in press (1996)	Aug. 1995
803	Riahi, D. N.	On the structure of an unsteady convecting mushy layer	Aug. 1995
804	Meleshko, V. V.	Equilibrium of an elastic rectangle: The Mathieu–Inglis–Pickett solution revisited—*Journal of Elasticity* **40**, 207-238 (1995)	Aug. 1995
805	Jonnalagadda, K., G. E. Kline, and N. R. Sottos	Local displacements and load transfer in shape memory alloy composites	Aug. 1995
806	Nimmagadda, P. B. R., and P. Sofronis	On the calculation of the matrix–reinforcement interface diffusion coefficient in composite materials at high temperatures—*Acta Metallurgica et Materialia*, in press (1996)	Aug. 1995
807	Carlson, D. E., and D. A. Tortorelli	On hyperelasticity with internal constraints—*Journal of Elasticity*, in press (1996)	Aug. 1995
808	Sayre, T. L., and D. N. Riahi	Oscillatory instabilities of the liquid and mushy layers during solidification of alloys under rotational constraint—*Acta Mechanica*, in press (1996)	Sept. 1995
809	Xin, Y.-B., and K. J. Hsia	Simulation of the brittle-ductile transition in silicon single crystals using dislocation mechanics	Oct. 1995
810	Ulysse, P., and R. E. Johnson	A plane-strain upper-bound analysis of unsymmetrical single-hole and multi-hole extrusion processes	Oct. 1995
811	Fried, E.	Continua described by a microstructural field—*Zeitschrift für angewandte Mathematik und Physik*, in press (1996)	Nov. 1995
812	Mittal, R., and S. Balachandar	Autogeneration of three-dimensional vortical structures in the near wake of a circular cylinder	Nov. 1995
813	Segev, R., E. Fried, and G. de Botton	Force theory for multiphase bodies—*Journal of Geometry and Physics*, in press (1996)	Dec. 1995
814	Weaver, R. L.	The effect of an undamped finite-degree-of-freedom "fuzzy" substructure: Numerical solutions and theoretical discussion	Jan. 1996
815	Haber, R. B., C. S. Jog, and M. P. Bensøe	A new approach to variable-topology shape design using a constraint on perimeter—*Structural Optimization* **11**, 1-12 (1996)	Feb. 1996